SENSITIVITY OF NORMALIZED DIFFERENCE VEGETATION INDEX (NDVI) ESTIMATION TO VARIOUS ATMOSPHERIC VARIABLES

A thesis submitted to the School of Graduate Studies
Addis Ababa University

In partial Fulfilment of the Requirements for the
Degree of Master of Science in Physics

By

Titike kassa

Addis Ababa, Ethiopia

July 2007

ADDIS ABABA UNIVERSITY
FACULTY OF SCIENCE
DEPARTMENT OF PHYSICS

The undersigned hereby certify that they have read and recommended to the Faculty of Science School of Graduate Studies for acceptance a thesis entitled "**SENSITIVITY OF NORMALIZED DIFFERENCE VEGETATION INDEX (NDVI) ESTIMATION TO VARIOUS ATMOSPHERIC VARIABLES**" by **Titike kassa** in partial fulfillment of the requirements for the degree of **Master of Science in Physics**.

Name	Signature
Dr. Gizaw Mengistu, Advisor	_____
Dr. Esayas Belay , Examiner	_____
Prof. A. V. Gholap , Examiner	_____

To you and the stones.

Acknowledgements

I would like to thank Dr. Gizaw Mengistu, my supervisor, for his many suggestions and constant support during this research. I will never forget silesh and his family support because he was always the base for my successes. I should also mention that my graduate studies in AAU were supported in part by the ministry of Education. Of course, I am grateful to my parents for their patience and *love*. Without them this work would never have come into existence (literally). *hima If I know what love is it is because of you*, you were always been with me.

Finally, I wish to thank the following: Abebe habite (for his friendship and support); sileshi (for changing my life from worse to bad); biyzinlgn, fantahun, samuel, birhanu, belay, desalegne, abera, Ermias, rehima, tige mariam, meqaunenit, chemeda ,yedne, abireham, taguna, seyife, samirawit, mihiret ... (for all the good and bad times we had together); giruminesh, asdesach (for special effects); hima and the Stones (they know why); *and* my adapted mam (for her love and care).

Addis Ababa, Ethiopia Titike Kassa

Abstract

A vegetation and atmospheric radiative method is employed to study different atmospheric parameter effect on vegetation index. Spectral and angular distribution of surface reflectance at different altitude of the atmosphere were simulated for different solar zenith angle. Sensitivity of normalized difference vegetation index (NDVI) to aerosol loading, cirrus cover, air mass and bidirectional reflectance distribution function (BRDF) has been studied. The result of the simulation for selected surface types have shown that NDVI increases with solar zenith angle irrespective of land surface types. More over our analysis reveals that sensitivity of NDVI to aerosol is highly pronounced for all surface types. The results are consistent with the expected physics of radiative transfer theory.

Table of Contents

List of Figures

Introduction

The normalized vegetation index (NDVI) has been widely used in optical remote sensing as a descriptor of vegetation. It is highly correlated with vegetation parameters such as green-leaf biomass and green-leaf area and, hence, is of considerable value for vegetation discrimination [1].

One of the primary interests of the Earth Observing System (EOS) program is to study the role of terrestrial vegetation in large-scale global processes with the goal of understanding how the Earth functions as a system. This requires an understanding of the global distribution of vegetation types as well as their biophysical and structural properties and spatial/temporal variations. Remote sensing observations offer the opportunity to monitor, quantify, and investigate large scale changes in vegetation in response to human actions and climate. Vegetation influences the energy balance, climate, hydrologic, and biogeochemical cycles and can serve as a sensitive indicator of climatic and anthropogenic influences on the environment. NDVI provide consistent, spatial and temporal comparisons of local and global vegetation conditions that will be used to monitor the Earths terrestrial photosynthetic vegetation activity for phenologic, change detection, and biophysical derivation of radiometric and structural vegetation parameters. Satellite remote sensing vegetation index (VI) products will play a major role in several EOS studies as well as be an integral part in the

production of many global and regional biospheric models and biogeochemical cycles. Currently, satellite-derived vegetation indices are being integrated in interactive biosphere models as part of global climate modelling [2] and production efficiency models [3]. They are also used for a wide variety of land applications, including natural resource management, agriculture, the Global Health and Human Monitoring Program, and operational Famine Early Warning Systems [4, 5]. This latter example is one of the few examples where derived satellite data are currently being used to drive policy decisions.

However NDVI is a controversial vegetation index. Because of its ratio form, it is susceptible to the variations in atmospheric conditions, surface conditions, topography, and sensor characteristics, none of which have any relationship to vegetation. This problem makes it difficult to derive meaning through the comparison of multitemporal NDVI maps. Therefore, satellite images should be preprocessed to remove atmospheric effects before they are compiled to develop NDVI images. A successful application of atmospheric correction algorithms require a sound understanding of radiometric process in the atmosphere. In this study we will investigate the physical process by which atmospheric conditions affect NDVI estimation using Moderate Resolution Atmospheric Radiance and Transmittance Model (MODTRAN) radiative transfer simulation code. Chapter 1 deals with radiative transfer in earth atmospheric system; Chapter 2 presents remote sensing and canopy radiative transfer modeling; Chapter 3 discuses overview and background information of NDVI; Chapter 4 discuses different atmospheric parameter effect on NDVI ; and Chapter 5 covers result and discussion.

Chapter 1

Radiative transfer in earth system

In this chapter we will discuss radiative transfer in earth atmospheric system with emphasis on components of at sensor radiance and physical parameter that are used to determine radiance components.

1.1 Total at-sensor radiance and its components

Total at the sensor radiance comprises of all reflected and path radiation getting in to sensor field of view. Symbolically, it can be written as

$$L_\lambda^{TOA} = L_\lambda^u + L_\lambda^{dif} + L_\lambda^p \tag{1.1.1}$$

where L_λ^{TOA} is total at sensor radiance, L_λ^u is unscattered component, L_λ^{dif} is diffused (sky irradiance) and L_λ^p is path scattered radiance component.

$$L_\lambda^{TOA} = \rho(x,y,\lambda)\frac{\tau_\nu(\lambda)}{\pi}\{\tau_s(\lambda)E_\lambda^0 cos[\theta(x,y)] + F(x,y)E_\lambda^{dif}\} + L_\lambda^p \tag{1.1.2}$$

The radiance observed from a down-looking sensor is comprised of many components, as illustrated in (Fig. 1.1). Typically, the quantity to be determined from these measurements is the spectrally dependent surface reflectance function or albedo. For a

near-infrared (NIR) and visible (VIS) sensor such as moderate resolution spectro radiometer (MODIS), the dominant contribution to the observed radiance is the surface scattered sun light. In the limit in which atmospheric attenuation and scattering are negligible, the reflectance function is simply the ratio of the observed spectral radiance to the solar spectral irradiance (the normalized ratio includes a factor of π steradians over the cosine of the solar zenith angle). In reality, other radiance components and atmospheric absorption are present. The data correction usually involves forward calculations with a comprehensive radiative transport model such as MODTRAN.
The basic approach in MODTRAN is to approximate the atmosphere and Earth surface as a sequence of quasihomogeneous layers for which the individual layer radiance contributions from each of the source terms depicted in Fig.(1.1) is considered. The surface is treated as a layer of infinite opacity, an opaque boundary with variable emissivity/reflectivity. Spherical refraction geometry effects are incorporated into calculation of path sums and scattering angles, although multiple scattering radiances are based on plane-parallel models. Approximate corrections are made for the effects of inhomogeneous distributions of temperature and species concentrations within the atmospheric layers.

The atmospheric effect on spectral radiance consists of two main mechanisms, scattering and absorption. Scattering is mainly due to the presence of particles in the atmosphere, while absorption comes about due to the energy transfer from the optical radiation to molecular motion of atmospheric gases. Both of these effects are wavelength dependent. From (fig. 1.1), several main factors are seen to contribute to the radiance received by the sensor.

The spectral irradiance on the top of the atmosphere E_λ^0, can be calculated using

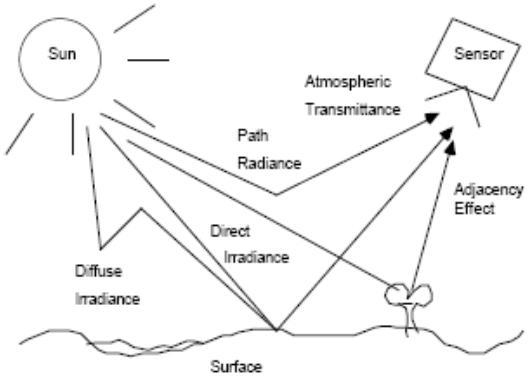

Figure 1.1: Atmospheric Effects on Spectral Radiance Received by Sensor.

Planck's equation and a few geometrical terms. It varies by only a couple of percent depending on the distance between the sun and earth. E_λ^0 is attenuated and scattered by the atmosphere before reaching the surface as the direct spectral irradiance E_λ^{dir}. Some of scattered radiation also reaches the surface as a diffuse spectral irradiance (or skylight irradiance), E_λ^{dif}. The direct spectral irradiance E_λ^{dir}, passes through the atmosphere and is attenuated by the spectral transmittance τ_λ of the atmosphere before it reaches the surface. Also, some of the solar irradiance that is scattered by the atmosphere finds its way into the sensor field of view as the path spectral radiance, E_λ^p. This path radiance also includes that which may have been reflected off of the nearby surface (adjacency effect) before being scattered into the sensor field of view, as well as the background radiation of the atmosphere. Direct irradiance E_λ^{dir} mathematically can be described by

$$E_\lambda^{dir}(x,y) = \tau_s(\lambda) E_\lambda^0 \cos\theta(x,y) \tag{1.1.3}$$

It is dependant on the solar path atmospheric transmittance $\tau_s(\lambda)$ as well as the zenith angle θ by way of the cosine rule. The solar path atmospheric transmittance

$\tau_s(\lambda)$ is a function of the distance the solar beam travels through the atmosphere (which is a function of solar zenith angle θ) as well as atmospheric parameters which influence scattering, absorption and transmittance.

Surface reflected unscattered component, L_λ^{un} can be derived from the irradiance at the earths surface. The irradiance downward onto a *lambertian* surface is converted in to the radiance leaving the surface with the aid a geometric factor π:

$$L_\lambda^{un}(x,y) = \rho(x,y,\lambda)\frac{E_\lambda^{dir}}{\pi} \tag{1.1.4}$$

where ρ is bidirectional reflectance distribution function,

Now we can account for the radiance leaving the surface and traveling through the atmosphere L_λ^u towards the sensor:

$$L_\lambda^u = \tau_\nu(\lambda)L_\lambda^{un} \tag{1.1.5}$$

Thus the total surface reflected unscattered component can be rewritten using (1.1.3), (1.1.4) and (1.1.5) as

$$L_\lambda^u = \rho(x,y,\lambda)\frac{\tau_\nu(\lambda)\tau_s(\lambda)E_\lambda^0}{\pi}cos[\theta(x,y)] \tag{1.1.6}$$

The diffused (sky radiance) that reaches the sensor can be given as

$$L_\lambda^{dif} = F(x,y)\rho(x,y,\lambda)\frac{\tau_\nu(\lambda)E_\lambda^{dif}}{\pi} \tag{1.1.7}$$

where F is fraction of the sky hemisphere which is visible from a pixel of interest.
Path scattered component, L_λ^p is one of radiance reaching the sensor before coming to the surface of the earth. It is a function of the amount of Rayleigh, Mie and non

selective scattering in the atmosphere. It is highly dependent on wave length and is assumed to be constant over a scene.

Now combining L_λ^{dif}, L_λ^u, with L_λ^p on the basis of relation derived in (1.1.6) (1.1.7), we arrive at (1.1.2)

The bidirectional reflectance distribution function (BRDF) ρ given in (1.1.4) is the ratio of the reflected intensity $I_{\lambda r}^+$, to the energy in the incident beam I_λ^-. As such, ρ is a function of wavelength (λ), incident angle $(\Omega)'$, and scattered angle (Ω)

$$\rho(\lambda, -\hat{\Omega}', \hat{\Omega}) = \frac{dI_{\lambda r}^+(\hat{\Omega})}{I_\lambda^-(\hat{\Omega}')\cos\theta' d\hat{\Omega}'} \tag{1.1.8}$$

The reflected intensity in any particular direction $\hat{\Omega}$ is the sum of contributions from all incident directions $\hat{\Omega}'$ that have a finite probability of reflecting into $\hat{\Omega}$.

$$\begin{aligned} I_{\lambda r}^+(\hat{\Omega}) &= \int_{-\hat{\Omega}'} dI_{\lambda r}^+(\hat{\Omega}) \\ &= \int_{-\hat{\Omega}'} I_\lambda^-(\hat{\Omega}')\rho(\lambda, -\hat{\Omega}', \hat{\Omega})\cos\theta' d\hat{\Omega}' \end{aligned} \tag{1.1.9}$$

The dependence of $\rho(\lambda, -\hat{\Omega}', \hat{\Omega})$ on two directions and on frequency makes it a difficult property to measure.

Fortunately many surfaces found in nature obey simpler reflectance properties first characterized by Lambert. A *Lambertian surface* is one whose reflectance is independent of both incident and reflected directions. The reflectance of a Lambertian surface depends only on wavelength

$$\rho(\lambda, -\hat{\Omega}', \hat{\Omega}) = \rho_L(\lambda) \tag{1.1.10}$$

The intensity reflected from Lambertian surface is given by

$$\begin{aligned} I^{+}_{\lambda r}(\hat{\Omega}) &= \int_{-\hat{\Omega}'} I^{-}_{\lambda}(\hat{\Omega}')\rho_L(\lambda)\cos\theta' d\hat{\Omega}' \\ &= \rho_L(\lambda)F^{-}_{\lambda} \end{aligned} \tag{1.1.11}$$

This shows as that, the intensity reflected from a Lambertian surface depends only on the incident irradiance, F^{-}_{λ} and not at all on the details of the angular distribution of the incident intensity field. The irradiance reflected from a Lambertian surface F^{+}_{λ} is the cosine-weighted integral of the reflected intensity (1.1.11) over all reflected angles

$$\begin{aligned} F^{+}_{\lambda r} &= \int_{\hat{\Omega}} I^{+}_{\lambda r}(\hat{\Omega})\cos\theta d\hat{\Omega} \\ &= \int_{\hat{\Omega}} \rho_L(\lambda)F^{-}_{\lambda}\cos\theta d\Omega \end{aligned} \tag{1.1.12}$$

Neither F^{-}_{λ} and $\rho_L(\lambda)$ depend on the emergent angle so the integral reduces to the familiar integral of $\cos\theta$ over the hemisphere so that

$$F^{+}_{\lambda r} = \pi\rho_L(\lambda)F^{-}_{\lambda} \tag{1.1.13}$$

The reflected irradiance may not exceed the incident irradiance or the requirement of energy conservation will be violated. Therefore (1.1.13) shows that

$$\rho_L(\lambda) \leq \pi^{-1} \tag{1.1.14}$$

with equality holding only for a perfectly reflective (non-absorbing) Lambertian surface. Many researchers prefer the Lambertian BRDF to have an upper limit of 1,

not π^{-1} (1.1.14). Thus it is common to encounter in the literature BRDF defined as $r = \pi\rho$.

1.2 Albedo

Land surface albedo is a critical parameter affecting the earths climate and is required by global and regional climatic modeling and surface energy balance monitoring.

Albedo can be represented as α; it is integral of BRDF (1.1.8)

$$\alpha_I(\theta_i, \lambda) = \int_0^1 \int_0^{2\pi} \rho(-\theta_i, \theta, \phi)\mu d\mu d\phi \tag{1.2.1}$$

where $\mu = cos\theta$ and $\rho(-\theta_i, \theta, \phi)$ is the bidirectional reflectance distribution function (BRDF). BRDF is the sole measure of surface reflectivity at the viewing direction given specific direct illuminations. Albedo defined above referred to us directional-hemispherical reflectance. Spectral apparent albedo ρ_A is defined as the ratio of upwelling irradiance $F_u(\theta_i; \lambda)$ to downward irradiance $F_d(\theta_i; \lambda)$ at the solar zenith angle θ_i:

$$\alpha_A(\theta_i; \lambda) = \frac{F_u(\theta_i; \lambda}{F_d(\theta_i; \lambda)} = \frac{\frac{1}{\pi}\int_0^1 \int_0^{2\pi} \int_0^1 \int_0^{2\pi} \rho(-\mu', \mu, \phi', \phi) L^{inc}(-\mu', -\mu_i, \phi', \phi_i)\mu\mu' d\mu d\mu' d\phi d\phi'}{\int_0^1 \int_0^{2\pi} L^{inc}(-\mu', -\mu_i, \phi', \phi_i)\mu' d\mu' d\phi'}, \tag{1.2.2}$$

where $L^{inc}(-\mu', -\mu_i, \phi', \phi_i)$ is the total downward radiance (direct plus diffuse) illuminated to the surface; it is obviously a function of the atmospheric conditions.

Chapter 2

Remote sensing and radiative transfer model of vegetation

In this chapter we will discuss about remote sensors, we apply our knowledge of chapter one to simulate transmittance and reflectance spectra and we will also discuss physical model of canopy radiative transfer.

2.1 Introduction to remote sensing

Remote sensing is the science of obtaining and interpreting information from a distance, using sensors that are not in physical contact with the object being observed. Though we may not realize it, we are familiar with many examples. Our eyes detect electromagnetic energy in the form of visible light. Some research suggests that migrating birds can sense variations in Earths magnetic field, which helps explain their remarkable navigational ability. The science of remote sensing in its broadest sense includes aerial, satellite, and spacecraft observations of the surfaces and atmospheres of the planets in our solar system, though the Earth is obviously the most frequent target of study. The term is customarily restricted to methods that detect and measure electromagnetic energy, including visible light, that has interacted with surface

materials and the atmosphere. Remote sensing of the Earth has many purposes, including making and updating planimetric maps, weather forecasting, and gathering military intelligence. Our focus in this work will be on remote sensing of resources of the earth especially the vegetation.

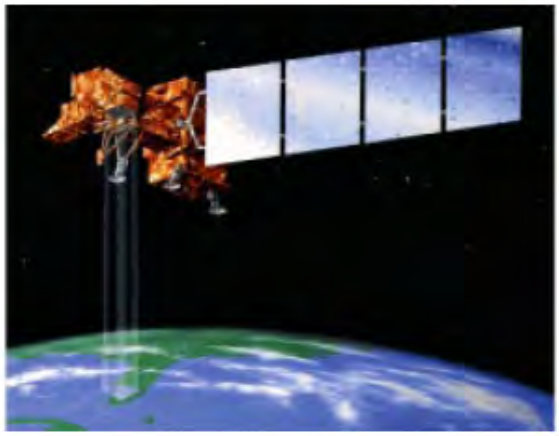

Figure 2.1: Landsat 7 satellite in orbit

2.2 Interaction processes in remote sensing

To understand how different interaction processes impact the acquisition of aerial and satellite images, let us analyze the reflected solar radiation that is measured at a satellite sensor. As sunlight initially enters the atmosphere, it encounters gas molecules, suspended dust particles, and aerosols. These materials tend to scatter a portion of the incoming radiation in all directions, with shorter wavelengths experiencing the strongest effect. Preferential scattering of blue light in comparison to green and red light which accounts for the blue color of the daytime sky. Clouds appear opaque because of intense scattering of visible light by tiny water droplets. Although most

of the remaining light is transmitted to the surface, some atmospheric gases are very effective at absorbing particular wavelengths. Example of this category is the absorption of dangerous ultraviolet radiation by ozone. As a result of these effects, the illumination reaching the surface is a combination of highly filtered solar radiation transmitted directly to the ground and more diffuse light scattered from all parts of the sky, which helps illuminate shadowed areas. As this modified solar radiation reaches the ground, it may encounter soil, rock surfaces, vegetation, or other materials that absorb a portion of the radiation. The amount of energy absorbed varies in wavelength for each material in a characteristic way, creating a sort of spectral signature. Most of the radiation left from absorption is diffusely reflected (scattered) back up into the atmosphere, some of it in the direction of the satellite. This upwelling radiation undergoes a further round of scattering and absorption as it passes through the atmosphere before finally being detected and measured by the sensor. If the sensor is capable of detecting thermal infrared radiation, it will also pick up radiation emitted by surface objects as a result of solar heating.

Scattering and absorption of EM radiation by the atmosphere have significant effects that impact sensor design as well as the processing and interpretation of images. When the concentration of scattering agents is high, scattering produces the visual effect we call haze. Haze increases the overall brightness of a scene and reduces the contrast between different ground materials. A hazy atmosphere scatters some light upward, so a portion of the radiation recorded by a remote sensor, called *path radiance*, is the result of this scattering process. Since the amount of scattering varies with wavelength, so does the contribution of path radiance to remotely sensed images. As shown by fig (2.3) below, the path radiance effect is greatest for the shortest

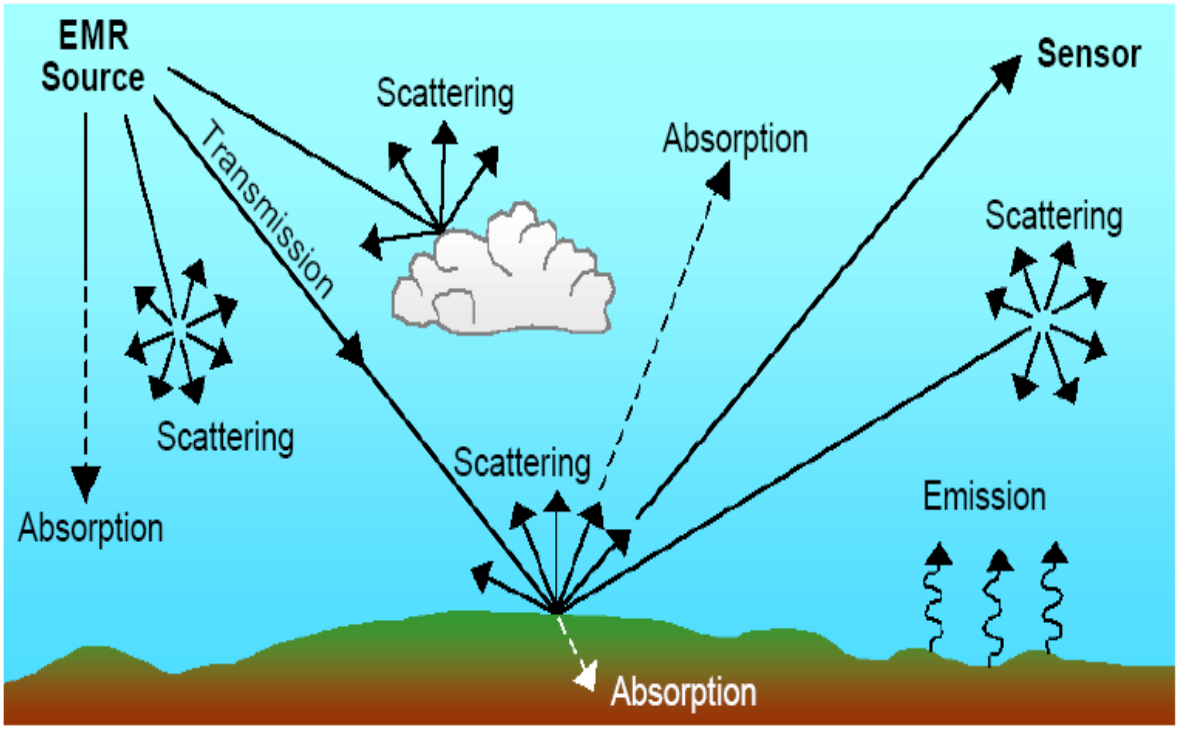

Figure 2.2: Typical EMR interactions in the atmosphere and at the Earths surface.

wavelengths, falling off rapidly with increasing wavelength. When images are captured over several wavelength ranges, the differential path radiance effect complicates comparison of brightness values at the different wavelengths. The atmospheric components that are effective absorbers of solar radiation are water vapor, carbon dioxide, and ozone. Each of these gases tends to absorb energy in specific wavelength ranges. Some wavelengths are almost completely absorbed. Consequently, most broad-band remote sensors have been designed to detect radiation in the atmospheric windows, those wavelength ranges for which absorption is minimal, and, conversely, transmission is high.

Scattering increases with increasing humidity and particulate load but decreases with

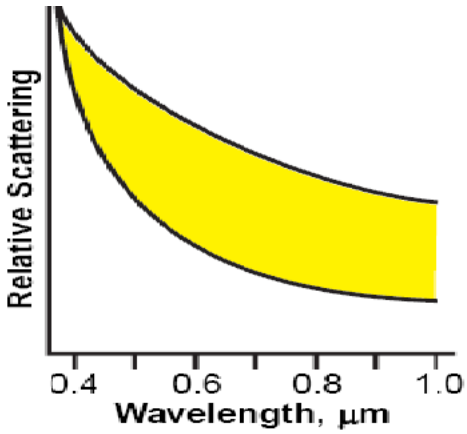

Figure 2.3: Range of scattering for typical atmospheric conditions (colored area) versus wavelength.

increasing wavelength. In most cases the path radiance produced by scattering is negligible at wavelengths longer than the near infrared.

2.2.1 Optical remote sensors

These sensor systems detect solar radiation that has been diffusely reflected (scattered) upward from surface features. The wavelength ranges that provide useful information include the ultraviolet, visible, near infrared and middle infrared ranges. Reflected solar sensing systems discriminate materials that have differing patterns of wavelength-specific absorption, which relate to the chemical make-up and physical structure of the material. Because they depend on sunlight as a source, these systems can only provide useful images during daylight hours, and changing atmospheric conditions and changes in illumination with time of day and season can pose interpretive problems. Reflected solar remote sensing systems are the most common type used to monitor Earth resources,

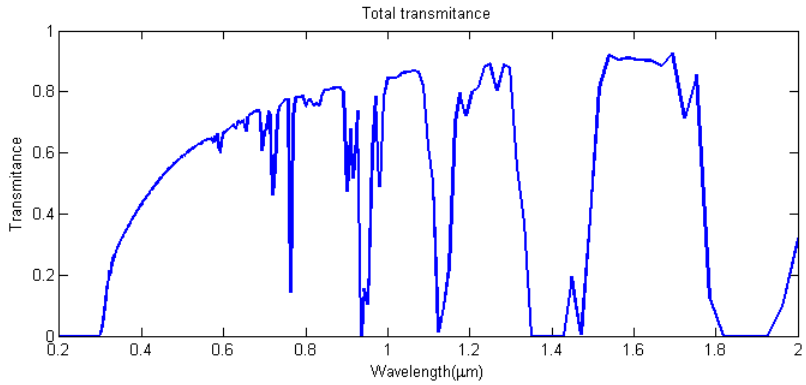

Figure 2.4: Variation in atmospheric transmission with wavelength of EM radiation, due to wavelength-selective absorption by atmospheric gases. Only wavelength ranges with moderate to high transmission values are suitable for use in remote sensing.

2.2.2 Spectral Signatures

The spectral signatures produced by wavelength-dependent absorption provide the key to discriminating different materials in images of reflected solar energy. The property used to quantify these spectral signatures is called spectral reflectance: the ratio of reflected energy to incident energy as a function of wavelength. The spectral reflectance of different materials can be measured in the laboratory or in the field, providing reference data that can be used to interpret images. As an example, the illustration below shows contrasting spectral reflectance curves for seven very common natural materials: dry bare soil, green grass, ocean water, old grass, dry grass, alfalfa and wheat. The reflectance of dry soil rises uniformly through the visible and near infrared wavelength ranges, peaking in the middle infrared range. It shows only minor dips in the middle infrared range due to absorption by clay minerals. Green vegetation has a very different spectrum. Reflectance is relatively low in the visible range, but is higher for green light than for red or blue, producing the green color

we see. The reflectance pattern of green vegetation in the visible wavelengths is due to selective absorption by chlorophyll, the primary photosynthetic pigment in green plants. The most noticeable feature of the vegetation spectrum is the dramatic rise in reflectance across the visible-near infrared boundary, and the high near infrared reflectance. Infrared radiation penetrates plant leaves, and is intensely scattered by the leaves complex internal structure, resulting in high reflectance. The dips in the middle infrared portion of the plant spectrum are due to absorption by water. Deep clear water bodies effectively absorb all wavelengths longer than the visible range, which results in very low reflectivity for infrared radiation.

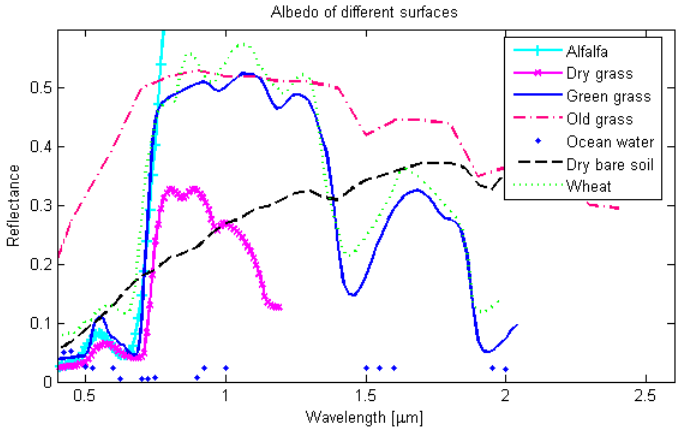

Figure 2.5: Spectral signature of different surfaces.

2.3 Modeling canopy reflectance

2.3.1 Introduction

In this section we will try to describe optical canopy reflectance (CR) modeling. This section describes the development of CR modeling methods for simulating the radiometric response of vegetation observed by a remote sensing instrument. Such models allow understanding of canopy radiometric processes and facilitate the inversion of canopy parameters from remotely sensed data.

2.3.2 Why we need to develop models of canopy reflectance

Models of optical canopy reflectance ρ_{canopy} have been developed for the purpose of understanding canopy radiometric behavior. If a model of canopy reflectance can be developed which satisfactorily (to some pre-defined level of accuracy) describes the variation in observed reflectance of the canopy under varying structural and radiometric conditions, then such a model can be used to interpret remotely sensed observations of a vegetation canopy. In addition, if such a model can be inverted (analytically or numerically) then estimates of the parameters driving the model may be determined from observations. This aim has driven much of the development in optical canopy reflectance modeling over the last two decades [26, 27]. Much of this modeling work has grown out of attempts to model and understand the reflectance of the Earth's surface.

Further more Vegetation plays an extremely important role in the global climate [28], providing a primary mechanism for the exchange of O2 and CO2 in the atmosphere, as well as energy fluxes through photosynthetic activity [29, 30], moisture fluxes [31] and transfers of momentum. For these reasons, much emphasis has been placed on

attempting to understand how vegetation can be detected and monitored from remote sensing measurements. One of the primary ways in which this has been achieved has been the development and refinement of CR modeling techniques.

2.3.3 Directional reflectance, the remote sensing signal and vegetation

Radiation reflected from the Earths surface is characterized by five signatures (or domains of information). reflectance transmittance and absorptance response of canopy elements to radiation of different wavelengths is one of canopy signal. These are related to spectrum, spatial features, temporal evolution, reflectance anisotropy and polarization effects. Spatial structure at the macroscopic level (objects are much larger than the wavelength of incident radiation), arrangement of scattering objects on a surface, appearance of target at different scales, adjacency, mixed pixels are also useful spatial features that enables us to discriminate different signals in remote sensing image. Temporal changes (e.g. seasonal change of vegetation growth profiles; inter-annual variability of vegetation quantity [32] can also serve as one of signatures. Reflectance anisotropy caused by surface structure (e.g. hotspot), the peak of reflectance in retro-reflection direction (where the viewing and illumination vectors and are near coincident. $\theta_{v,i}$, and $\phi_{v,i}$ are the viewing and illumination zenith and azimuth angles).

Polarization information contained in surface reflectance signal can be used for simplification of the problem. A sixth signature can potentially be identified - time-resolved returns from active optical (laser) sensors such as Light Detection And Ranging (LiDAR). LiDAR is currently being explored as a new method of obtaining information on surface properties, particularly vegetation canopy structure . Considering the

reflectance signal from a vegetation canopy, extends the description given above to propose the following functional description of the relationship, R, between the measured spectral directional reflectance ρ of a vegetation canopy, and the parameters controlling that signature:

$$\rho_{canopy} = R(\lambda, t, (x, y), (\Omega, \Omega'), p, c) \tag{2.3.1}$$

where λ, is wavelength, t is temporal, (x,y) spatial description of the scene, (Ω, Ω') illumination and viewing direction of respectively, C is canopy parameter. In addition to the five signatures described above, R is also dependent on a set of canopy parameters, representing the characteristics of the canopy and its underlying surface (soil, snow etc.) contributing to the form of ρ_{canopy}. In order to derive information regarding vegetation from measurement of reflectance, models of vegetation canopy reflectance are constructed . CR modeling attempts to i) formulate an accurate forward relationship to predict ρ_{canopy} for given R; and ii) determine C from measured ρ_{canopy} at given values of $\lambda, t, (x, y), (\Omega, \Omega'), p$ i.e. to invert (or understand) the canopy parameters from the relationship in equation .

2.4 Factors affecting surface directional reflectance

The size, shape and distribution of objects on a surface have a direct impact on the nature of the radiation scattered from the surface . The measured reflectance signal is therefore a function of surface structure. Vegetation is one of the most important absorbing/scattering land surfaces that can impact a remote sensing signal [33]. The influence of vegetation is described through biophysical parameters such as leaf area index (LAI), fraction of absorbed photosynthetically active radiation

(fAPAR) and albedo (α). Ecologists, climatologists and remote sensing scientists use such parameters to relate the quantity and influence of vegetation on global climate processes.

It is well-known that natural surfaces are generally not Lambertian reflectors (i.e. angular distribution of reflected incident radiation is not the same in all directions), but will tend to display varying degrees of anisotropy. Surface reflectance is therefore not only a function of the spectral, spatial and polarizing properties of the target, but also of the direction from which the surface is illuminated and viewed. Measured reflectance (as opposed to the intrinsic surface reflectance) will also be dependent on the spectral and directional nature of the irradiance. CR modeling seeks to relate the information contained in observed reflectance to the structural and radiometric properties of the surface vegetation.

The degree to which incident radiation from a surface is reflected anisotropically is determined by factors such as the density and arrangement of objects on the surface, and hence the nature of the shadowing caused by these objects as a function of viewing and illumination zenith and azimuth angles, $\theta_{v,i}$, and $\phi_{v,i}$ respectively, as well as the intrinsic directionality of the reflectance, transmittance and absorptance properties of the scattering materials. Reflectance anisotropy can also be a function of the aggregated scattering properties of objects. The existence of surface structure tends to cause the surface to depart from Lambertian and, as a result, incident radiation is reflected more strongly in some directions than others. This directionality of surface reflectance can potentially be exploited to provide information regarding the surface structure. The hotspot peak, for example, arises because a minimum of shadowed surface is viewed when the viewing and illumination vectors are collinear. This is a

characteristic feature of vegetation canopy reflectance and is related to the size and distribution of scattering objects within the canopy. Surface reflectance anisotropy is described by the BRDF (1.1.8) [34]

The directional nature of the reflectance of the Earth's surface has been introduced, as well as some of the factors that cause observed variations in directional reflectance. The importance of vegetation as a source of these variations has also been discussed. The following sections provide an overview of the physical modelling technique that have been developed for interpreting the directional reflectance of vegetated surfaces for remote sensing studies. Canopy reflectance(CR) ρ_{canopy}, is known to be sensitive to a number of factors. These can be broadly divided into two categories: structural and radiometric.

Vegetation components such as leaves and stems are radiometrically characterized by their reflectance ρ and transmittance τ [35]. A complete canopy, on the other hand, is an aggregation of individual scattering objects. Total ρ_{canopy} depends on the nature of this aggregation, described by structural properties such as the area density, as well as the angular and spatial distribution (clumping) of scattering elements within the canopy. In addition to being a function of canopy (and atmospheric) parameters ρ_{canopy} will also be a function of the lower boundary beneath the canopy e.g. soil, snow, leaf litter etc. This boundary has its own radiometric and structural properties (microscopic and macroscopic roughness) which may contribute to the measured reflectance signal.

2.5 Physical model

A great deal of effort has been devoted to development of physically-based models of surface scattering [36, 37]. A primary advantage of using physical models is that they are based on physical processes and so their parameters will have some physical meaning. It is also often possible to make reasonable a priori estimations of the model parameters and to constrain them to physically realistic values during inversion. Particularly attention is paid to radiative transfer (RT) and geometric optic (GO) models of reflectance. In a complex physical system such as that of photon interaction with vegetation, often the only effective way to achieve a manageable and tractable representation of the system is to make approximations.

Typical requirements of a physical CR model are:

- to represent (selected/all) scattering features of the canopy in the spatial, spectral and angular domains.

- to relate observed reflectance behavior to the controlling biophysical parameters sufficiently well such that these parameters may be derived from measured reflectances through model inversion; and

- to allow generalizations of theoretical treatments of canopy scattering based on observed scattering behavior.

The following section describes some of the approaches that have been taken to simplify the physical approach to CR modelling

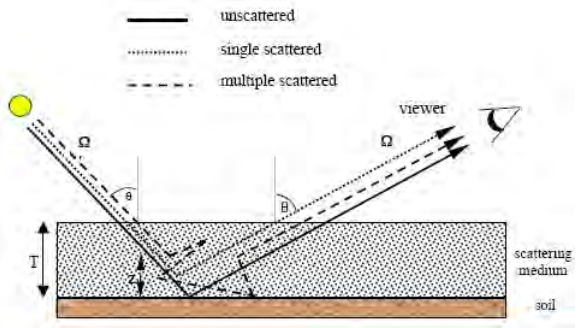

Figure 2.6: Schematic representation of the turbid medium approximation, showing the various scattered components of excitant radiation.

Canopy reflectance of the turbid medium and radiative transfer (RT)

One of the most powerful tools used in modelling canopy scattering behavior is that of radiative transfer. RT theory was developed by Chandrasekhar as a method describing radiation transport in the gaseous clouds formed during stellar evolution. Chandrasekhar's idea has since been modified and applied in many fields, including canopy reflectance modelling. In this approach the canopy is approximated as a layer (or layers) of infinitely extended, plane-parallel homogenous scattering medium consisting of randomly oriented infinitesimal scattering phytoelements (leaves). This so-called 'turbid medium' approach is illustrated in fig.(2.6). The assumption of the canopy as a turbid medium allows a number of approximations and simplifications to be made regarding canopy scattering behavior.

The turbid medium approach has proved a powerful technique modelling photon transport in vegetation canopies and has been applied widely to the problem. The radiance field resulting from single and multiple scattered photon interactions (see fig.2.6) can be described by considering the conservation of energy within each canopy

layer, and specifying the sources of radiation external to that layer (boundary conditions).

The result is an integro-differential equation describing the change in intensity along a viewing direction Ω due to i) scattering interactions causing radiation to be scattered out of the illumination direction Ω' (sink term), and ii) interactions causing radiation to be scattered from other directions into the direction Ω (source term). If the so-called far-field approximation is made [38] whereby scattering elements are assumed to be infinitesimal and there is no mutual shadowing (and polarization, frequency shifting interactions and emission are disregarded) the problem of upward and downward energy fluxes within the canopy can then be represented as a solution of the well-known radiative transfer equation i.e.,

$$-\mu\frac{\partial I(z,\Omega)}{\partial z} = -\sigma_e(z,\Omega)I(z,\Omega) + \int_{4\pi}\sigma_s(z,\Omega'\rightarrow\Omega)I(z,\Omega')d\Omega' \qquad (2.5.1)$$

$I(z,\Omega)$ is the specific energy intensity at a height z within a horizontal plane-parallel canopy of total height T ($0 < z < T$) (so $\frac{\partial I(z,\Omega)}{\partial z}$ is the steady-state radiance distribution function); σ_e is the extinction coefficient of the canopy medium; σ_s is the differential scattering coefficient for photon scattering from direction the illumination direction Ω' into a unit solid angle about the viewing direction Ω.

This problem has been studied extensively in astrophysics, planetary astronomy, particle physics and neutron transport among other fields, and many methods are available for its solution under certain conditions. To solve equation (2.5.1) for a vegetation canopy, approximations regarding σ_e and σ_s are often made [39]. One of the most powerful approximations used in modeling reflectance behavior is to concentrate on

single scattering interactions within the canopy. Single scattering interactions are in most cases the dominant component of ρ_{canopy} [40], particularly at visible wavelengths. Considering single scattering interactions within a turbid medium, the radiation intensity in the incident direction, Ω', at a depth z within the canopy can be described using Beer's law (Beer- Lambert law):

$$I(\Omega', z) = I(\Omega', 0)exp(\frac{-L(z)G(\Omega')}{\mu'}) \tag{2.5.2}$$

$I(\Omega', 0)$ is the direct irradiance incident on the top of the canopy; L(z) is the downward cumulative LAI in the canopy at depth z (m^2m^{-2}). This is actually $u_l(z)$, the leaf area density (one-sided leaf area per unit volume of canopy at depth z in the canopy in (m^2m^{-3})) integrated over all z. $G(\Omega')$ is the leaf projection function i.e. the fraction of leaf area projected in the illumination direction Ω'; μ' is the cosine of the illumination zenith angle, θ_i. $G(\Omega)$, the leaf projection function (in the viewing direction), is defined as

$$G(\Omega) = \frac{1}{\pi}\int_{2\pi+} g_l(\Omega_l)|\Omega_l.\Omega|d\Omega_l \tag{2.5.3}$$

where $g_l(\Omega_l)$ is the angular distribution of the leaf normals, Ω_l i.e. leaf angle distribution (LAD). $g_l(\Omega_l)$ is typically assumed to be spherical for simplicity i.e. all leaf orientations are equally probable Although this is a widely used assumption, it can cause inaccuracies. Beers law as stated is for a perfectly homogeneous canopy, and the LAI parameter takes no account of the possibility of vegetation being clumped. This is highly unlikely in practice . If LAI is redefined as effective LAI/Le, then a true LAI can be defined as $L = Le/\kappa$, where κ is a clumping index. If $\kappa > 1$ then leaves are regularly dispersed within the canopy e.g. row crops; if $\kappa = 1$ then leaves

are dispersed randomly; if $\kappa < 1$ then the canopy is clumped dense patches of vegetation interspersed with voids (gaps between the clumps). As clumping increases, Le decreases, and the probability of gaps in the canopy increases leading to a higher soil reflectance for given LAI.

The assumption of the turbid medium, along with the approximations required to derive Beers law, permits a description of the single scattering radiance field within a vegetation canopy as a function of a small number of simple structural parameters. A normalized leaf scattering phase function, $\Gamma(\Omega' \rightarrow \Omega)$, describing the angular distribution of scattering (from the illumination direction Ω' into the viewing direction, Ω) at each photon interaction (c.f. σ_s in equation (2.5.1)) and a joint gap probability, $Q(\Gamma(\Omega' \rightarrow \Omega), z)$, can be derived. Q describes the probability of existence of free lines of sight to the top of the canopy for a photon traveling from Ω' to Ω at a depth z within the canopy. Clearly, if a photon is unable to make it both down and back up to the top of the canopy, it will not emerge to be available for measurement (without further scattering). If the far-field approximation is made, then $Q(\Gamma(\Omega' \rightarrow \Omega), z)$ is simply the probability of photons traveling a distance z/μ' in direction Ω', multiplied by the probability of traveling z/μ in the direction Ω'. The individual gap probabilities in the downward and upward paths can be calculated according to Beers law (2.5.2).

Chapter 3

Overview and background information of vegetation indices

3.1 Vegetation indices

Many studies have shown the relationships of red and near-infrared (NIR) reflected energy to the amount of vegetation present on the ground. Reflected red energy decreases with plant development due to chlorophyll absorption within actively photosynthetic leaves. Reflected NIR energy, on the other hand, will increase with plant development through scattering processes (reflection and transmission) in healthy, turgid leaves. Unfortunately, because the amount of red and NIR radiation reflected from a plant canopy and reaching a satellite sensor varies with *solar irradiance*, *atmospheric conditions*, *canopy background*, and *canopy structure/ and composition*, one cannot use a simple measure of reflected energy to quantify plant biophysical parameters nor monitor vegetation on a local or global, operational basis. This is made difficult due to the intricate radiant transfer processes at both the leaf level (cell constituents, leaf morphology) and canopy level (leaf elements, orientation, non photosynthetic vegetation (NPV), and background). This problem has been circumvented somewhat by combining two or more bands into an equation or vegetation

index(VI).

The simple ratio (SR) was the first index to be used [6], formed by dividing the NIR response by the corresponding red band output,

$$SR = \frac{\rho_{nir}}{\rho_{red}} \tag{3.1.1}$$

where ρ can be digital counts, at- satellite radiances, top of the atmosphere apparent reflectances, land leaving surface radiances, surface reflectances, or hemispherical spectral albedos. However, for densely vegetated areas, the amount of red light reflected approaches very small values and this ratio, consequently, increases without bounds. [7] normalized this ratio from -1 to +1, with the normalized difference vegetation index (NDVI), by ratioing the difference between the NIR and red bands by their sum:

$$NDVI = \frac{\rho_{nir} - \rho_{red}}{\rho_{nir} + \rho_{red}} \tag{3.1.2}$$

For terrestrial targets the lower boundary became approximately zero and the upper boundary approximately 0.80.

As a vegetation monitoring tool, the NDVI is utilized to construct seasonal, temporal profiles of vegetation activity enabling interannual comparisons of these profiles. The temporal profile of the NDVI has been shown to depict seasonal and phenologic activity, length of the growing season, peak greenness, onset of greenness, and leaf turnover or 'dry-down' period. [8] presented a 10 year NDVI data record of northern Boreal forests showing a warming trend whereby the length of the growing season

had increased by nearly 2 weeks. They showed the usefulness of such NDVI growing season plots for change detection and monitoring. [9] similarly used NDVI seasonal profiles to show desert expansions and contractions in the Sahara. The time integral of the NDVI over the growing season has been correlated with net primary production (NPP).

Many studies have shown that NDVI is related to leaf area index (LAI), green biomass, percent green cover, and fraction of absorbed photosynthetically active radiation (fAPAR) [10, 11, 12, 13, 14]. Relationships between fAPAR and NDVI have been shown to be near linear [15, 16], in contrast to the non-linearity experienced in LAI NDVI relationships with saturation problems at LAI values over 2. Other studies have also shown that NDVI is related to carbon-fixation, canopy resistance, and potential evapotranspiration allowing its use as input to models of biogeochemical cycles [17, 18, 19].

The current procedure for generation of composited, AVHRR-based, NDVI products is the maximum value composting (MVC) technique. This is accomplished by selecting, on a pixel by pixel basis, the input pixel with the highest NDVI value as output to the composited product. The procedure generally includes cloud screening and data quality checks. Since residual cloud cover, not accounted for in the cloud masking procedure, and atmospheric sources of contamination both lower NDVI values, a maximum NDVI would select the least cloud- and atmospheric-contaminated pixels. Furthermore, since the influence of atmospheric contamination and residual cloud cover increases with optical path length, the maximum NDVI criterion also has a tendency to select the most near-nadir view and smallest solar zenith angle pixels (least

optical path lengths), thus standardizing to a certain degree the variable sun-surface-sensor observation geometries over a composting cycle. The MVC works nicely over near-Lambertian surfaces where the primary source of pixel variations within a composite cycle is associated with atmosphere contamination and path length, however, its major shortcoming is that the anisotropic, bi-directional influences of the surface is not considered. The bidirectional spectral behavior of numerous, global land cover types and terrestrial surface conditions have been widely documented and shown to be highly anisotropic due to canopy structure, shadowing, and background contributions. Ratioing of the NIR and red spectral bands to compute vegetation indices does not remove surface anisotropy due to the spectral dependence of the BRDF response. The atmosphere counteracts and dampens the surface BRDF signal, mainly through the increasing path lengths associated with off-nadir view angles and/or sun angles.

The maximum NDVI value selected is thus, related to both the bidirectional properties of the surface and the atmosphere, which renders the MVC-based selection unpredictable. The MVC favors cloud free pixels, but does not necessarily pick the pixel closest to nadir or with the least atmospheric contamination. Although the NDVI tends to increase for atmospherically corrected data, it does not mean that the highest NDVI is an indication of the best atmospheric correction. Many studies have shown the MVC approach to select off-nadir pixels with large, forward-scatter (more shaded) view angles and large solar zenith angles, which are not always cloud-free or clear atmosphere [20, 21]. This degrades the potential use of the VI for consistent and accurate comparisons of global vegetation types.

3.2 Theoretical description of vegetation indices

The theoretical basis for empirical-based vegetation indices is derived from examination of typical spectral reflectance signatures of leaves (Fig. 3.1). The reflected energy in the visible is very low as a result of high absorption by photosynthetically active pigments with maximum sensitivity in the blue (470 nm) and red (670 nm) wavelengths. Nearly all of the near-infrared radiation is scattered (reflected and transmitted) with very little absorption, in a manner dependent upon the structural properties of a canopy (LAI, leaf angle distribution, leaf morphology). As a result, the contrast between red and near-infrared responses is a sensitive measure of vegetation amount, with maximum red - NIR differences occurring over a full canopy and minimal contrast over targets with little or no vegetation (Fig. 3.1). For low and medium amounts of vegetation, the contrast is a result of both red and NIR changes, while at higher amounts of vegetation, only the NIR contributes to increasing contrasts as the red band becomes saturated due to chlorophyll absorption.

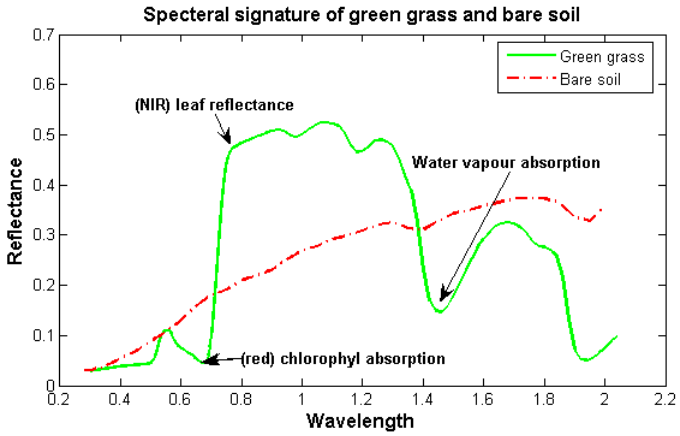

Figure 3.1: Spectral reflectance signature of a photosynthetically active leaf with a soil signature to show contrast

The red-NIR contrast can be quantified through the use of ratios (NIR/red), differences (NIR-red), or hybrid approaches of the above. Vegetation indexes are measures of this contrast and thus are integrative functions of canopy structural [% cover, LAI (leaf area index), LAD(leaf area density)] and physiological (pigments, photosynthesis) parameters. The contrast between red and NIR canopy reflectances for a variety of canopy types and canopy backgrounds may also be depicted in graphical form, using the red and near-infrared reflectances as axes. In such a plot, a triangular, cloud of points is observed with well-defined boundaries, whether the data plotted are temporally variable reflectances of agricultural crops over the growing season (Fig. 3.2) or spatially variable reflectances of different land covers from desert to forests (Fig. 3.3).

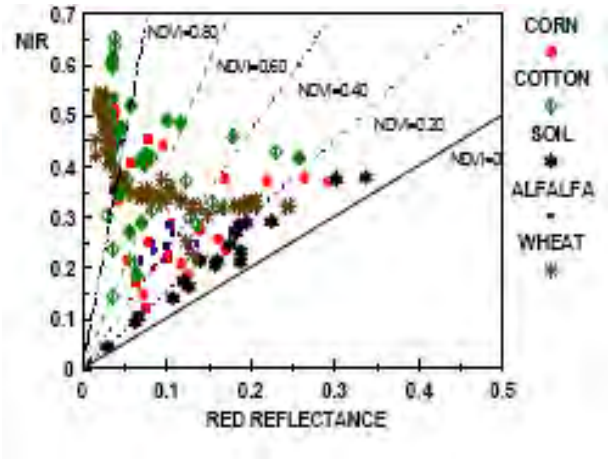

Figure 3.2: Cloud of reflectance points in NIR-red waveband space for agricultural crops observed throughout the growing season.

In both cases there is a lower baseline of pixels close to the 1:1 line, representing the lower boundary condition of vegetation. This baseline boundary condition can

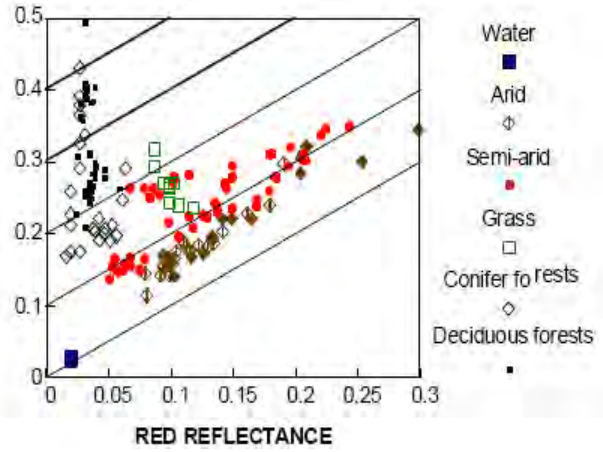

Figure 3.3: Cloud of reflectance points in NIR-red reflectance space from Landsat TM for a wide range of land surface cover types.

be further extended to include water targets (dark), snow backgrounds (bright), soils with variable mineralogies and litter and detrital material at variable stages of decomposition (bright to dark) or incorporation into the dark soil humus pool. The basic premise of the lower baseline is that only non-photosynthetic targets with low contrast in the red and NIR will occupy this area. The third apex represents dense vegetation which is at or close to the lowest red values (chlorophyll-absorption) and highest NIR values. Note, the lower baseline involves non-photosynthetic canopy backgrounds and would not include a separate understory canopy, i.e., multiple canopy layers are all treated as overlying canopy and not background. Pixels with increasing amounts of green vegetation shift away from the lower baseline toward the apex of maximum NIR and low red reflectance in a manner dependent upon the optical/ structural properties of the vegetation canopy and the optical properties of the canopy background (soil, snow, water, understory, etc.) (Fig. 3.2). The greater the amount of green vegetation present in a pixel, the greater will be the red-NIR contrast, and thus the shift away

from the lower baseline. In (Fig. 3.3), desert regions fall near the lower zero baseline, followed by semi-arid and grassland pixels. Closed forest canopies and open forests with green understories occupy the extreme left-hand portion, varying very little in the red (saturation) with larger variations along the NIR axis (Fig. 3.2), in accordance with expected optical behavior. The pixels inside the triangular cloud structure are generally mixed pixels, with multiple responses from the vegetation and background components. Over 70% of the Earths terrestrial surface is classified as open canopies with mixed background and vegetation signals. The role of vegetation indices is to model the behavior and boundary conditions of the cloud of terrestrial-based pixels in NIR-red space and their associated variations in time and space. Within the cloud of spectra we can identify pairs of red and NIR reflectances which represent equal amounts of a particular vegetation parameter. This may be described by the term "vegetation isoline" and may be derived via canopy radiative transfer models and/or observational data sets. Vegetation Index isolines, on the other hand, represent all combinations of red and NIR reflectance responses resulting in the same VI value. These are the model parameters which dissect the pixel data structure into various levels of vegetation amounts. They create the gray levels of the vegetation index from low to high. The concept of isolines essentially connect radiative transfer theory with vegetation indices and provide a basis for decoupling atmosphere and background signals from the vegetation signal

3.2.1 Theoretical basis of NDVI

The NDVI is a normalized transform of the NIR to red reflectance ratio, ρ_{nir}/ρ_{red} , designed to standardize VI values to between -1 and $+1$;

$$NDVI = \frac{[(\rho_{nir}/\rho_{red}) - 1]}{[(\rho_{nir}/\rho_{red}) + 1]} \tag{3.2.1}$$

As a ratio, the NDVI has the advantage of minimizing certain types of bandcorrelated noise (positively-correlated) and influences attributed to variations in direct/diffuse irradiance, clouds and cloud shadows, sun and view angles, topography, and atmospheric attenuation. Ratioing can also reduce, to a certain extent, calibration and instrument-related errors. The NDVI, as a ratio, can be computed from raw digital counts, top-of-the-atmosphere radiances, apparent reflectances (normalized radiances), and partially or total atmospheric corrections. Although the units cancel out, the NDVI values themselves change so one must be consistent in how the NDVI is derived. The extent to which ratioing can reduce noise is dependent upon the correlation of noise between red and NIR responses and the degree to which the surface exhibits Lambertian behavior. Ratios create simple, red-NIR space, vegetation index isolines of increasing slopes diverging out from the origin, i.e., slopes increase with vegetation amount and intercepts are independent of vegetation amount with a constant value of zero. The NDVI efficiently shows increasing values from the baseline region to the green apex. Furthermore, the large range in background brightness values, with little or no vegetation present, fall close to the 1:1 line showing that the NDVI is able to ratio out a significant portion of these spectral variations with NDVI values constrained to values slightly above zero. The robustness of the NDVI is well established. As long as nonvegetation sources of spectral variation cause pixels to shift toward or away the origin, it is following an NDVI isoline or equal NDVI value. The NDVI is the only VI currently adapted to global processing and it is used extensively in global, regional, and local monitoring studies. It has also been used

on a wide array of sensors and platforms from Landsat TM(thematic mapper), to the NOAA-AVHRR series, MODIS and ground-based radiometers. In the following sections, we try to analyze sensitivity of NDVI to various atmospheric effect. Up to now the burden of noise removal in satellite data is placed on the NDVI equation itself and thus the NDVI has the task of minimizing noise and simultaneously enhancing vegetation signals. The remotely-sensed spectral signatures, however, vary with both external and internal factors such as sensor calibration, atmosphere, sun- and view angles, and canopy background. Because of these influences, VIs also show variations which result in inaccuracies in estimating vegetation biophysical parameters. As advancements are made in minimizing many of the external influences, such as sensor calibration, noise removal, atmosphere correction, and BRDF modeling, other nonratioing approaches, including canopy models, may be used to better depict vegetation spatial and temporal variations.

Chapter 4

Sensitivity of NDVI to various atmospheric parameters

In this chapter we will discus about effects of different atmospheric parameters in estimation of NDVI.

4.1 Atmospheric effect

The atmosphere degrades the NDVI value by reducing the contrast between the red and NIR reflected signals. The red signal normally increases as a result of scattered, upwelling path radiance contribution from the atmosphere while the NIR signal tends to decrease as a result of atmospheric attenuation associated with scattering and water vapor absorption. The net result is a drop in the NDVI signal and an underestimation of the amount of vegetation at the surface. The degradation of NDVI signal is dependant on aerosol content of the atmosphere, with the turbid atmospheres resulting in the lowest NDVI signals. The impact of the atmospheric effect on NDVI value is most serious with aerosol scattering (0.04-0.02), water vapor (0.04 - 0.08), and rayleigh scattering (0.02 -0.04) [22]. Atmospheric effect on the NDVI will become minimal by implementing the atmospheric correction algorithm prior to NDVI computation.

4.2 BRDF effect

The NDVI has been shown to be affected by variations in bidirectional reflectances resulting from differences in sun-target-sensor geometries. The strong anisotropic properties from vegetation canopies seriously affect vegetation indices, an effect that will differ from sensor to sensor e.g anisotropic properties become more pronounced with MODIS data in which atmosphere correction will further enhance surface-based anisotropies, which vary with land cover type, relative amounts of characteristic vegetation and soil components, and sun-earth-sensor geometry. The resulting deviations must be considered in the derivation of the vegetation index products. This resulting variability in view and sun angles is important for the (seasonal and interannual) intercomparison of vegetative covers on a global basis. Therefore, some knowledge of the bi-directional reflectance distribution function (BRDF) is needed for successful utilization of directional reflectance data and vegetation indices, and the derivation of land cover-specific biophysical parameters [23].

The influence of variable sun-target-sensor configurations on derived vegetation indices can be standardized in various manners, including: (1) standarding reflectances to nadir view angle at a solar zenith angle representative of the observations; (2) standarding reflectances to nadir view angle and a temporally and globally constant solar zenith angle; (3) adjusting to a constant off-nadir view angle with a constant sun angle; or (4) using spectral (bi-hemispherical) albedos, we have chosen direct reflectances to nadir view angle and various solar zenith for estimation of NDVI.

4.3 Canopy background effect

In contrast to the previous sources of noise and uncertainty, this source of uncertainty is best handled in the formulation of the VI equation itself, since canopy background (soil, litter, snow, and water) effects on the VI are not readily corrected for prior to VI computation. Background effects are best removed within the VI equation itself because (1) they cannot be assessed independently as in atmosphere and BRDF; and (2) in validation, a true VI value for a given canopy is needed, one that does not depend upon the background optical properties. Numerous ground-, air-, and satellite-based observations have shown the NDVI to be overly sensitive to the brightness of the underlying canopy background, [24, 25]. Canopy backgrounds exhibit spatial and temporal reflectance variations resulting from rain events, snowfall, litterfall, roughness, and the organic matter content and mineralogy of the soil substrate material. In all of these studies there is a systematic increase in the NDVI value as the reflectance or brightness of the background decreases.

A common misconception is that canopy background considerations are only important in sparsely vegetated, arid and semi-arid areas, where spectral variations in background are the greatest. However, most studies and simulations show NDVI background sensitivity to be greatest at intermediate levels of vegetation, comparable to humid and sub-humid land cover types, including open forest stands.

4.4 Atmospheric gases effect

The processes of atmospheric scattering by aerosols and molecules, and absorption by gases (ozone, water vapor and carbon dioxide) disturb terrestrial surface reflectance

measurements acquired by optical satellites sensors. When designing remote sensing sensors, the spectral bands are selected in order to avoid as much as possible encroaching on the absorption bands of atmospheric gases. NDVI is calculated from the surface reflectance (albedo) measured by two bands in the red and near infrared as shown in Equation (3.2.1). As we have tried to explain in chapter two NDVI is highly affected by spectral band selection for NIR and RED bands of satellite remote sensors. Remote sensing people uses atmospheric windows(chanale/band) of solar spectrum for estimation of NDVI. But this windows(band) are affected by absorption of atmospheric gases, like water vapor,ozone,carbon dioxide. Absorption (primarily due to water vapor) is very much spectrally dependent. Thus, for an instrument designed to estimate NDVI, the specification of the bands are primarily determined by vegetation surface reflectance and atmospheric gases transmittance characteristics. In this study we have used moderate resolution spectral radiometer (MODIS) response function band1 ($0.64\mu m - 0.82\mu m$) for RED band and band2 ($0.819\mu m - 0.9\mu m$) for NIR for estimation of NDVI. In order to see the gaseous absorption effects on these spectral bands (red and near infrared) and, consequently on NDVI, radiative transfer code modtran3 used. A tropical atmosphere model with default concentration of these gases used, we fixed the view in nadir and the solar angle at 45^0. We have simulated using the transmittance code of MODTRAN3 to see altitudinal profile, and absorption band these gases so that we can select sensor position and spectral band which is not affecting estimation of NDVI. The Figure in chapter4 shows the spectral absorption by water vapor, ozone, carbon dioxide and their atmospheric profile that we simulated and show the spectral dependence of atmospheric gaseous absorption.

4.5 Atmospheric aerosol effect

Aerosols are a suspension of small solid and liquid particles in the atmosphere. These particles can reflect and absorb solar radiation, which is the aerosol direct effect. Aerosols can also modulate the radiative energy budget through their impact on cloud particle size, cloud liquid/ice water content, and cloud lifetime, which is the aerosol indirect effect. The aerosol radiative forcing is defined as the difference between the outgoing solar flux without aerosols and the flux with aerosols under clear-sky conditions. Aerosol particles play an important role in the earth's atmosphere system because of their direct interaction (absorption and scattering) with solar and terrestrial radiation. The aerosols have potential to warm or cool the earth's atmosphere system depending upon their absorptivity and surface albedo. The scattering and absorption properties of individual particles depend upon the particle shape, size, refractive index and wavelength of incident radiation. The radiative properties of an aerosol layer depend on the above factors as well as on the spatial distribution of the particles, angle of incidence of radiation, and for the nonspheric particles their orientation. However, the impact of aerosol layer is not only determined by its particle size distribution and composition, but also by its location and thickness in the atmosphere, the nature of the underlying surface and the presence of the clouds.

Aerosol scatters solar radiation before it reaches the surface and absorbs it again after it is reflected by the surface and before it reaches the satellite sensor [41]. Atmospheric aerosols (smoke, dust, and air pollution particles) have a significant effect on all of the vegetation indices, reducing the contrast between red and NIR reflectances, thus lowering vegetation index values, whether they are based on the NIR-red difference or

the NIR/red ratio. The atmospheric aerosol influences on VI in two ways: influence as path-radiance (additive effect), and influence through transmittance (multiplicative effect). The additive effect is determined regardless of the land surface (canopy-soil layers) brightness, thus has potential to be removed fairly well as demonstrated by several researchers[42]. On the other hand, the multiplicative effect depends on the surface brightness, hence its minimization becomes more complicated.

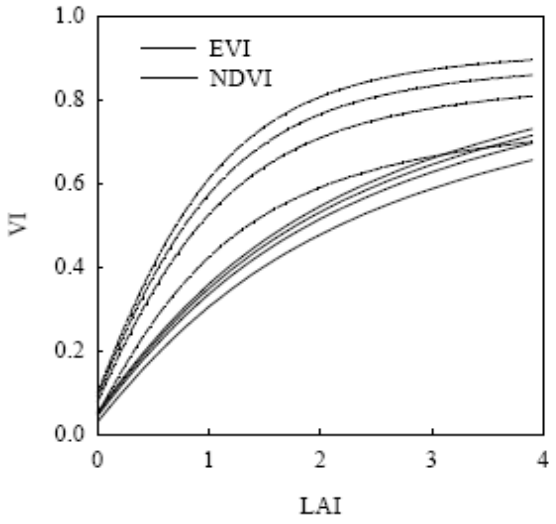

Figure 4.1: VI vs. LAI for different visibility with a constant soil brightness

(Figure 4.1) shows the vegetation index - LAI relationships for a set of simulated atmospheres of four visibility levels (100km, 20km, 10km, 5km) under the same aerosol type (continental aerosol model of 6S). The figure clearly shows differences in the VI-LAI relationships for the different visibility levels. There exists both direct and indirect correction methods, involving ground-based measurements, radiative transfer models, climatology, and dark object subtraction approaches. However, to date, correction for aerosols over land has never been achieved on an operational basis and

it may not be possible to implement a globally consistent, atmospheric correction scheme utilizing climatology and dark object subtraction methods. The second way is to use VIs stable to the atmospheric condition variations. There has been several vegetation index equations developed which minimize aerosol influences indirectly on a pixel by pixel basis. This would be useful in smoke-filled areas, where the spatial variability of aerosols will exceed the resolution grid size of the aerosol products.

MODTRAN: Its capacity and scope in simulating various effects on NDVI estimates MODTRAN has been widely used in different applications of satellite remote sensing and contains many important elements in radiative transfer codes. MODTRAN has been adopted by many researchers as one of radiative transfer code to derive surface reflectance from satellite measurements. The accuracy of The code is very important because any errors in the radiative transfer calculation will directly translate into errors in the derived surface reflectance. We have used MODTRAN3 for simulation of land surface reflectance shown in (Fig. 4.2). A total of 6 different surface reflectance spectra in the wave length range of $(0.2\mu m - 2\mu m)$, in tropical atmospheric model with the same solar zenith ($\theta_s = 50^0$) and nadir view angle and rural aerosol loading were input into MODTRAN3 in radiance code. Since angular dependencies of these surface reflectance spectra are not available, we simply assume these surface cover types are Lambertian (isotropic in reflectance).

So far, we have covered the model physics ,remote sensing of land surface resources, theoretical basis of NDVI and have reviewed established facts about the various effects on NDVI estimation. In the next chapter, we will employ simulation code to investigate the aforementioned effects viz atmospheric gases, aerosols, and sensor-target-solar geometries at the time of measurement.

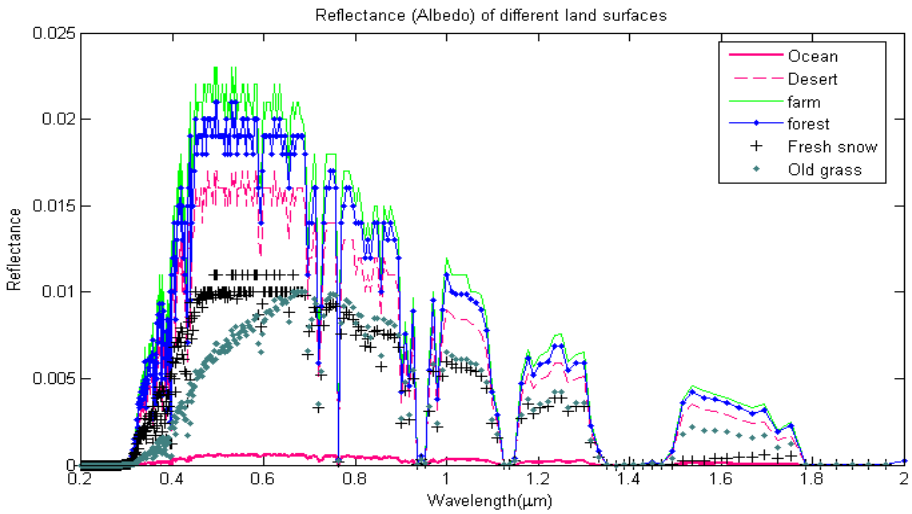

Figure 4.2: Surface reflectance spectra simulated from MODTRAN3.

Chapter 5

Results, discussion and conclusion

In this study we have tried to examine various atmospheric effect on estimation of NDVI. NDVI is proposed and used as best indicator of vegetation amount and condition in regional and global level. It is estimated using at- satellite radiances, land leaving surface radiances, surface reflectances, or hemispherical spectral albedos based on the principle that different land surface cover have reflectance signature in different band width of solar spectrum. We have used two MODIS vegetation channels in red ($0.614\mu m - 0.682\mu m$) and NIR ($0.819\mu m - 0.9\mu m$) bands. These band widths are selected because the absorption in these bands by atmospheric gases is minimal. The atmospheric model used in the study represents model atmosphere for tropical conditions. Fig 5.1 represents profiles of the three main absorbing gasses in the tropical atmosphere.

Fig 5.2 shows the signature of these gases in wave length band selected for NDVI estimation.

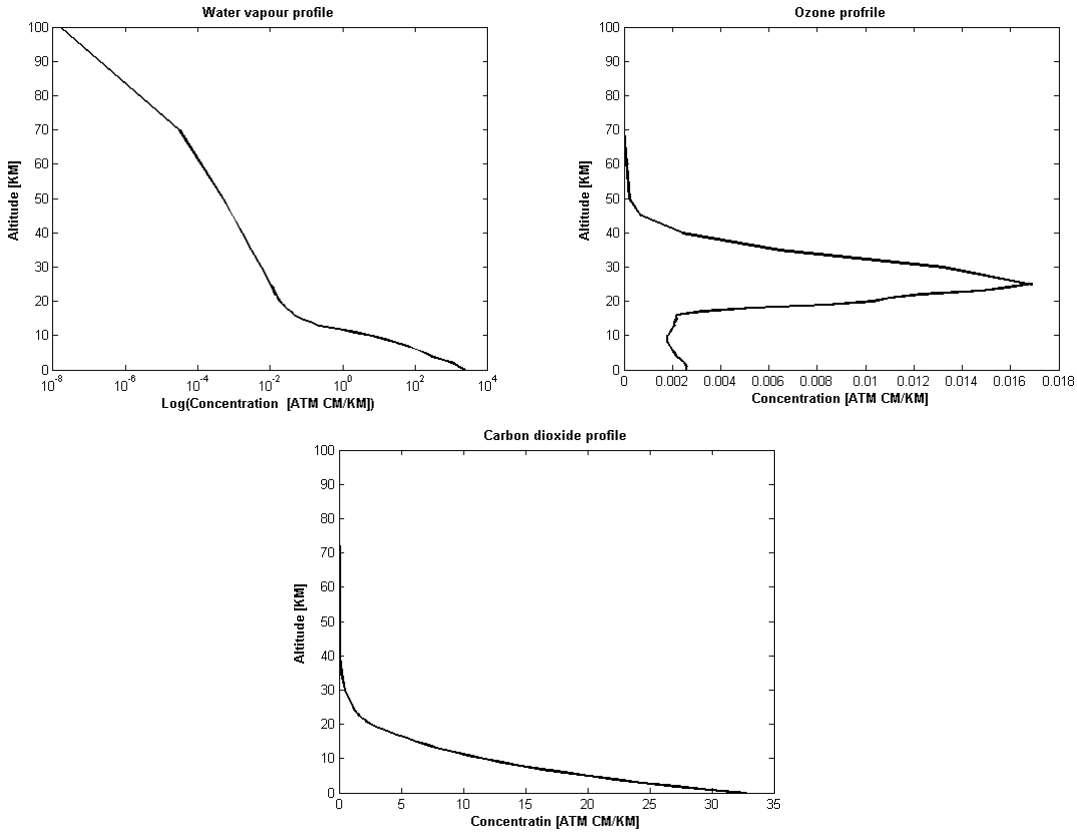

Figure 5.1: Left-top: Tropical atmosphere profile of water vapor; Right-top: Tropical atmosphere profile of Ozone; Bottom: Tropical atmosphere profile of carbon dioxide.

5.1 NDVI sensitivity to BRDF

Figs. 5.3 and 5.4 depicts the dependance of NDVI on the position of the Sun with respect to target surfaces. Fig 5.3 shows NDVI for forest land surface at different solar zenith angles. The simulation is performed by placing the sensor at an altitude of 0.2 km to avoid atmospheric effects. This altitude is nearly close to the surface which means that there is insignificant interference from atmospheric gasses in the atmospheric depth between the sensor and target surface.

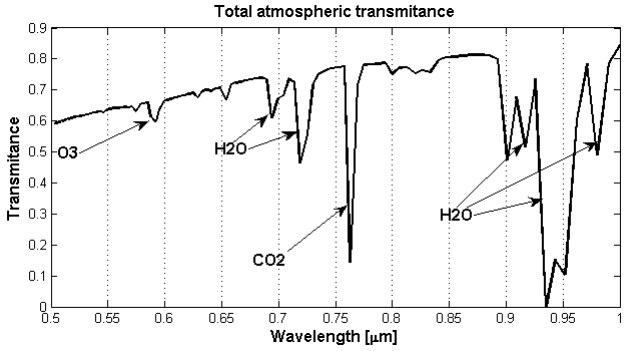

Figure 5.2: Total atmospheric Spectral Transmittance.

In the same Fig. 5.3, the effect of air mass is shown by placing the sensor at an altitude of 6 km. When the two curves in Fig. 5.3 is compared, on increase in NDVI is clearly observed over all solar zenith angles. However, the difference in NDVI between the two cases is more significant in high solar zenith angle than low solar zenith angle. In Fig. 5.4, similar investigation has been performed for a farm land surface as the target of the observation. NDVI estimate increases when the sensor is at 5.5 km as compared to sensor at 0.2 km. The change with solar zenith angle exhibits similar pattern observed for forest land surface.

The air mass factor is mainly linked with absorbing gasses in between sensor targets. This effect can be highly appreciated by investigating Fig. 5.5. Fig. 5.5 shows the effect of optical path length with respect to water vapor. The transmittance due to water vapor falls dramatically as the sensor moves from altitude of 0.2 km to 100 km. It is possible to examine the effects of other absorbing gases and particulate matter along the line of view of the sensor. In general, the response of NDVI is based on the assumption that variation in bidirectional factor is greatly a function of sun-target-sensor geometry.

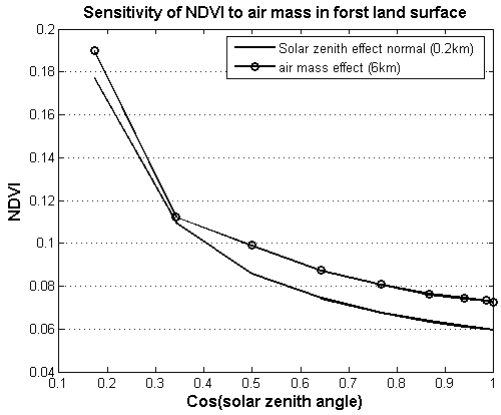

Figure 5.3: Air mass effect on NDVI in different altitude in forest land surface

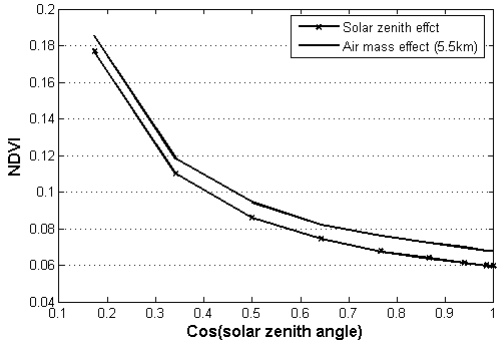

Figure 5.4: Air mass effect on NDVI in different altitude in farm land surface

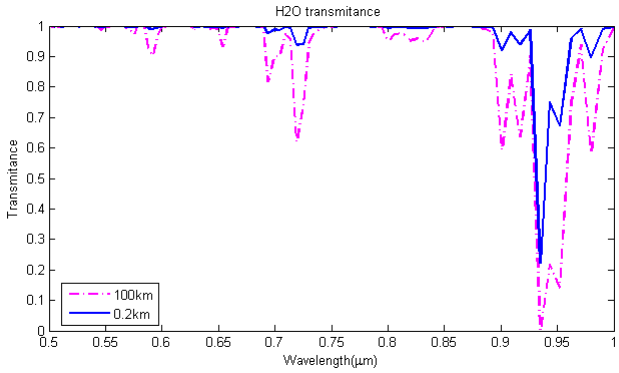

Figure 5.5: Effect of air mass on Spectral Transmittance of water vapor.

5.2 NDVI sensitivity to Aerosol

Aerosol has significant impact on the NDVI estimates due to its scattering and absorbing property. Fig. 5.6 (left and right panes) shows the influence of aerosols on NDVI estimation for forest and farm land surfaces. The aerosol effect is significant over all solar zenith angles for both land surfaces. However, the remarkable increase in NDVI at larger zenith angle for both land surfaces reveals that NDVI estimates when sun is near horizon is not reliable.

Aerosol and airmass effects on NDVI estimation are also assessed as shown in Fig. 5.7 for old grass land surface cover. The NDVI sensitivity to aerosol is higher than the air mass effect. The difference gets pronounced increasing solar zenith angle.

5.3 NDVI sensitivity to air mass

So far, we have determined sensitivity of NDVI to in all the discussion in section 5.1 and 5.2. Fig. 5.8 compares the NDVI sensitivity to aerosol, cirrus cover, air mass and BRDF for farm land surfaces. A remarkable feature that can be inferred from the

figure is that aerosol effect is the most important parameter to which NDVI responds appreciably.

The increment in NDVI values towards high solar zenith angle for all surface indicates that the direct solar radiance in the red band is highly attenuated along the optical path length which increases with increase in solar zenith angle. This also reveals that the impact on the near infrared is weak. When the air mass effect is incorporated, a further rise in NDVI value is noticed. At a given solar zenith angle, the NDVI is enhanced due to air mass. The increase in air mass will again allow for more red band to be attenuated. This means that if the sensor is placed at a higher altitude, the distance traveled by direct solar radiation on its way from the sun to the target and then back to the sensor will increase. Therefore, our simulation agrees with indications of fundamental radiative transfer theory.

The aerosol effect is highly pronounced and follows similar pattern with increase in solar zenith angles. The pronounced responses of NDVI to aerosol is an evidence for dominance of forward scattering in the direction of line of sight. Moreover, the near infrared band is scattered more than the red band in the forward directions. This agree with the aerosol size distribution used for this sensitivity study.

Fig. 5.9 illustrates the dependance of NDVI on solar zenith angle for three land surfaces. The variation of NDVI value for these surfaces are clearly indicated. The NDVI value of old grass is larger than that of farm and forest surfaces. However NDVI is the same for farm and forest surfaces which might be related to the difference in reflectance signature of these surfaces.

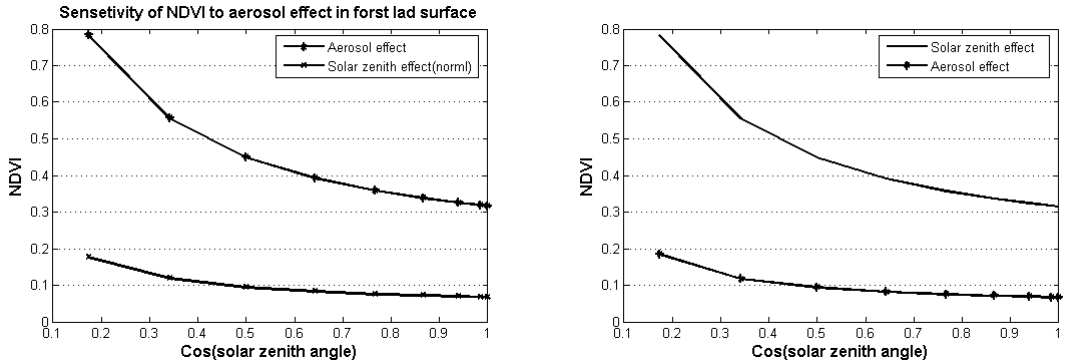

Figure 5.6: Left: Aerosol effect on NDVI in forst land surface; Right: Aerosol effect on NDVI in farm land surface.

5.4 conclusion

The effect of BRDF, air mass, aerosol, cirrus cover, on NDVI are examined. NDVI shows the sensitivity to these parameters. The aerosol effect is most significant over all solar zenith angles for all land surfaces. This is because its scattering absorbing properties in the atmosphere. air mass determining gaseous profile in the atmosphere is found important because the increased air mass causes the increase of radiance in near infrared band, but the decrease in red band. Consequently, successful atmospheric correction needs the accurate estimation of aerosol optical thickness, selective absorption by atmospheric gases and sun-target-sensor geometry. In near future, this study should be extended into the investigation of the combinational effect of parameters for selected area and developing algorithm that forecast NDVI for Ethiopia

.

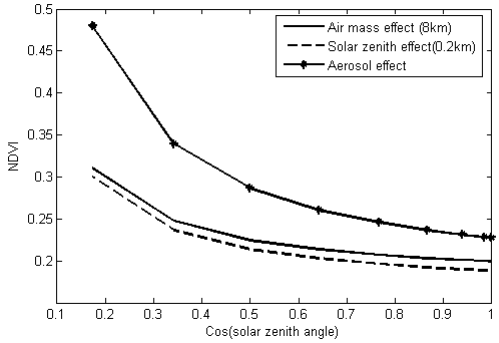

Figure 5.7: Sensitivity of NDVI to different atmospheric parameter in old grass land surface cover

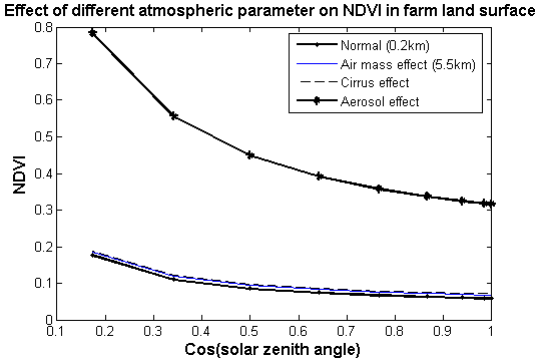

Figure 5.8: Sensitivity of NDVI to different atmospheric parameter in farm land surface cover

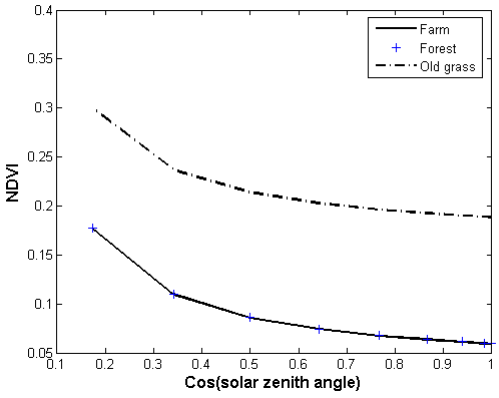

Figure 5.9: Solar zenith angle effect on NDVI for forest, farm and oldgrass land surfaces.

Bibliography

[1] C. O. Justice, J. R. G. Townshend, B. N. Holben, and C. J. Tucker, Analysis of the phenology of global vegetation using meteorological satellite data, Int. J. Remote Sens., vol. 6, pp. 12711318, 1985.

[2] Sellers, P. J., Tucker, C. J., Collatz, G. J., Los, S., Justice, C. O., Dazlich, D. A., and Randall, D. A. (1994), A global 1 * 1 NDVI data set for climate studies. Part 2 - The adjustment of the NDVI and generation of global fields of terrestrial biophysical parameters, *Int. J. Remote Sensing*, 15:3519-3545.

[3] Prince, S. D., Justice, C. O., and Moore, B. (1994), Remote Sensing of NPP, IGBP DIS Working Paper 10, IGBP-DIS, Paris.

[4] Prince, S. D. and Justice, C. O. (1991), (Editorial) Special issue on coarse resolution remote sensing of the Sahelian environment, *Int. J. Remote Sensing*, 12(6):1137-1146.

[5] Hutchinson, C. F. (1991), Use of satellite data for Famine Early Warning in sub-Saharian Africa, *Int. J. Remote Sensing,* 12(6):1405-1421.

[6] Jordan, C. F. (1969), Derivation of leaf area index from quality of light on the forest floor, *Ecology*, 50:663-666.

[7] Deering, D. W. (1978), Rangeland reflectance characteristics measured by aircraft and spacecraft sensors. Ph.D. Dissertation, Texas A and M University, College Station, TX, 338 pp.

[8] Myneni, R. B, Keeling, C. D., Tucker, C. J., Asrar, G., and Nemani, R. R. (1997), Increased plant growth in the northern high latitudes from 1981 to 1991, Nature 386:698-702.

[9] Tucker (1985) NDVI seasonal profiles to show desert expansions and contractions in the Sahara.

[10] Asrar, G., Fuchs, M., Kanemasu, E. T.,and Hatfield, J.L.(1984),Estimating absorbed Photosynthetic radiation and leaf area index from spectral reflectance in wheat,*Agron. J.*, 76:300-306.

[11] Baret, F. and Guyot, G . (1991), potentials and limits of vegetation indices for LAI APAR assessment , *remote sensing . Environ.*, 35: 161-173.

[12] Goward, S. N. and Huemmerich, K.F. (1992), vegetation canopy PAR absorptance and normalized difference vegetation index: an assessment using the SAIL model ,*Remote Sens. Environ.*, 39: 119 -140.

[13] Running, S. W. and Nemani, R. R. (1988), Relating seasonal patterns of the AVHRR vegetation index to simulated photosynthesis and transpiration of forest in different climates, *Remote Sens. Environ.*, 24:347-367.

[14] Curran, P. J. (1980), Relative reflectance data from preprocessed multispectral photography, *Int. J. Remote Sens.*, 1:77-83.

[15] Pinter, P. J., Jr. (1993), Solar angle independence in the relationship between absorbed PAR and remotely sensed data for alfalfa, *Remote Sens. Environ*, 46:19-25.

[16] Daughtry, C. S. T., Gallo, K. P., Goward, S. N., Prince, S. D., and Kustas, W. P. (1992), Spectral estimates of absorbed radiation and phytomass production in corn and soybean canopies, *Remote Sens. Environ,* 39:141-152.

[17] Raich, J. W. and Schlesinger, W. H. (1992), The global carbon dioxide flux in soil respiration and its relationship to vegetation and climate, Tellus, 44B:81-99.

[18] Running, S. W., Nemani, R. R., Peterson, D. L., Band, L. E., Potts, D. F., Pierce, L. L., and Spanner, M. A. (1989), Mapping regional forest evapotranspiration and photosynthesis by coupling satellite data with ecosystem simulation, *Ecology*, 70:1090-1101.

[19] Running, S. W. (1990), Estimating terrestrial primary productivity by combining remote sensing and ecosystem simulation, *In Ecological Studies Vol Remote Sensing of Biosphere Functioning*, H. Mooney and R. Hobbs., eds., Springer-Verlag, pp.65-86.

[20] Moody, A. and Strahler, A. H. (1994), Characteristics of composited AVHRR data and problems in their classification, *Int. J. Remote Sensing*, 15(17):3473-3491.

[21] Cihlar, J. C., Ly, H., Li, Z., Chen, J., Pokrant, H., and Huang, F. (1997), Multi temporal, multichannel AVHRR data sets for land biosphere studiesArtifacts and corrections, *Remote Sens. Environ.*, 60:35-57.

[22] Goward, S. N., Markham, B. L., Dye, D. G., Dulaney, W., and Yang, J. (1991), Normalized difference vegetation index measurements from the Advanced Very High Resolution Radiometer, *Remote Sens. Environ.*, 35:257-277.

[23] Cihlar, J., Manak, D., and DIorio, M. (1994a), Evaluation of Compositing Algorithms for AVHRR Data over Land, IEEE Trans. *Geosc. Remote Sens.*, 32:427-437.

[24] Huete, A. R. and Warrick, A. W. (1990), Assessment of vegetation and soil water regimes in partial canopies with optical remotely sensed data, Remote Sens. Environ., 32:155-167.

[25] Qi, J., Huete, A. R., Moran, M. S., Chehbouni, A., and Jackson, R. D. (1993a), Interpretation of vegetation indices derived from multi-temporal SPOT images, Remote Sens. Environ., 44:89-101.

[26] Asrar, G. Ed. (1989) Theory and applications of optical remote sensing, J. Wiley and Sons, New York.

[27] Goel, N. S. and Thompson, R. L. (2000) A snapshot of canopy reflectance models, and a universal model for the radiation regime, *Rem. Sens. Rev.*, 18, 197-225.

[28] Dickinson, R. E. (1983) Land surface processes and climate - surface albedos and energy balance, Adv. *Geophys.*, 25, 305-353.

[29] Ross, J. K. (1981) *The radiation regime and architecture of plant stands*, W. Junk, The Hague, Netherlands

[30] Verstraete, M. M. (1987) Radiation transfer in plant canopies: transmission of direct solar radiation and the role of leaf normal orientation, *J. Geophys. Res.*, 92, 10,985-10,995.

[31] Shukla, J. and Mintz, Y. (1982) Influence of land-surface evapotranspiration on the earth's climate, *Science*, 215, 1498-1501.

[32] Myneni, R. B., Keeling, C. D., Tucker, C. J., Asrar, G. and Nemani, R. R. (1997) Increased plant growth in the northern high latitudes from 1981 to 1991, Nature, 386 (6626), 698-702.

[33] Myneni, R. and Ross, J. (eds.) (1990) Photon-vegetation interactions: applications in optical remote sensing and plant ecology, Springer-Verlag, Heidelberg, Germany.

[34] Nicodemus, F. E., Richmond, J. C., Hsia, J. J., Ginsburg, I. W. and Limperis, T. (1977) Geometrical consideration and nomenclature for reflectance, Nat. Beaureau of Stand. Report, NBS MN-160, 52 pp., Washington, D.C (in Wolff et al., 1992).

[35] Jacquemoud, S. and Baret, F. (1990) PROSPECT - A model of leaf optical properties spectra, *Rem. Sens. Environ.*, 34(2), 75-91.

[36] Myneni, R. B., Gutshick, V. P., Asrar, G. and Kanemasu, E. T. (1988) Photon transport in vegetation canopies with anisotropic scattering, Parts II and IV, *Agric. For. Meteorol.*, 42, 17-40 and 101- 120.

[37] Myneni, R. B., Ross, J. and Asrar, G. (1989) A review on the theory of photon transport in leaf canopies, *Agric. For. Meteorol.*, 45, 1-153.

[38] Myneni, R. B., Asrar, G. and Gerstl, S. A. W. (1990) Radiative transfer in three-dimensional leaf canopies, *Transp. Theory Stat. Phys.*, 19, 205-250. itex361

Chandrasekhar, S. (1960) Radiative Transfer, Dover, New York, USA.

[39] Myneni, R. B., Maggion, S., Iaquinta, J., Privette, J. L., Gobron, N., Pinty, B., Kimes, D. S., Verstraete, M. M. and Williams, D. L. (1995) Optical remote sensing of vegetation: modelling, caveats and algorithms, Rem. Sens. Environ., 51, 169-188.

[40] Myneni, R. and Ross, J. (eds.) (1990) *Photon-vegetation interactions: applications in optical remote sensing and plant ecology*, Springer-Verlag, Heidelberg, Germany.

[41] Kaufman, Y. J. and Tanre, D. (1996), Strategy for direct and indirect methods for correcting the aerosol effect on remote sensing: from AVHRR to EOS-MODIS, *Remote Sens. Environ.*, 55:65-79.

[42] Myneni, R. B. and Asrar, G. (1993), Atmospheric effects and spectral vegetation indices, *Remote Sens. Environ*, 390-402.

Declaration

I hereby declare that this thesis is my original work and has not been presented for a degree in any other university. All sources of material used for the thesis have been duly acknowledged.

Name: Titike Kassa

Signature: .....

This thesis has been submitted for the examination with my approval as university advisor.

Name: Dr. Gizaw Mengistu

Signature: .....

Addis Ababa University

Department of Physics

July, 2007